Quasistable quantum vortex knots and links in anisotropic harmonically trapped Bose-Einstein condensates

Christopher Ticknor,[1,*] Victor P. Ruban,[2,†] and P. G. Kevrekidis[3,‡]
[1]*Theoretical Division, Los Alamos National Laboratory, Los Alamos, New Mexico 87545, USA*
[2]*Landau Institute for Theoretical Physics, RAS, Chernogolovka, Moscow Region 142432, Russia*
[3]*Department of Mathematics and Statistics, University of Massachusetts, Amherst, Massachusetts 01003-4515, USA*

(Received 11 March 2019; published 10 June 2019)

The long-time existence of topologically nontrivial configurations of quantum vortices in the form of torus knots and links in trapped Bose-Einstein condensates is demonstrated numerically within the three-dimensional Gross-Pitaevskii equation with an external anisotropic parabolic potential. We identify parametric domains of trap anisotropy, characterized by the axial over planar frequency ratio $\lambda \approx 1.5$–1.6, where the lifetime of such quasistationary rotating vortex structures is many hundreds of typical rotation times. This suggests the potential experimental observability of the structures. We quantify the relevant lifetimes as a function of the model parameters (e.g., λ) and initial condition parameters of the knot profile.

DOI: 10.1103/PhysRevA.99.063604

I. INTRODUCTION

Topological structures bearing vorticity have been long recognized as objects of high interest in hydrodynamics, optics, and condensed-matter physics [1–3]. Within the particular theme of atomic gases in the realm of Bose-Einstein condensates (BECs) [4–6], a pristine setting has been identified for the exploration of the properties of such structures. More specifically, the static and dynamical properties of quantized vortices have played a crucial role in a wide range of associated theoretical, numerical, and experimental studies; as only a small ensemble of relevant examples, we mention the reviews in [7–12].

A focal theme of interest within this nexus of topological charge, nonlinearity, and spatial confinement has been the study of vortex rings and simple filaments [13–31] whose interaction dynamics and even leapfrogging [32–34] have been considered. An even more demanding three-dimensional (3D) territory that has been less explored (especially so experimentally) is that of vortex knot structures. These have been examined mainly for a uniform density background (see [35–43] and references therein). Also, no experimental technique for producing knots and links in Bose-Einstein condensates has been developed, with the exception of the remarkable synthetic structures produced in spinor Bose-Einstein condensates [44,45]; see also [46] for a related theoretical and numerical proposal of vortex knot realizations in two-component BECs via coherent two-photon Raman transitions. The study of knots is especially interesting given their emergence in a wide range of physical contexts. These range from macroscopic shaken strands of rope [47] to microscopic strands of DNA [48] and from contexts such as fluids [38] to magnetic fields in plasmas [49].

Very recently in Ref. [50], based on the hydrodynamic approximation (with potential perturbations neglected), simple vortex knots were considered theoretically in trapped axisymmetric condensates characterized by an equilibrium ground state density profile $\rho(z, r)$. In particular, the stability of torus vortex knots under suitable conditions was predicted. Its preliminary numerical verification was undertaken very recently by one of the present authors (V.P.R.) [51] within the Gross-Pitaevskii equation, with the latter representing a suitable 3D model for a rarefied Bose gas at zero temperature. For a few sets of system parameters, long lifetimes for torus vortex knots, unknots, and links were indeed observed. On the other hand, it is important to highlight that the earlier systematic work of [41] (involving thousands of relevant simulations) predicted instability of all the types of knots examined in the homogeneous condensate cases considered therein.

In light of the above results, there is an important open question remaining: Can knot (or link) structures become dynamically robust in the presence of trapping? Here we examine this question in the context of variation of model parameters and initial condition parameters. The former are represented by the parametric exploration as a result, e.g., of the trap anisotropy, while the latter are induced by the variation of the vortical pattern initial locations. Given the generic rotation exhibited by knot patterns, we do not seek these as exact stationary solutions. Rather, we consider a large range of dynamical simulations where a perturbed initial configuration is evolved and the outcome of the evolution is assessed, attempting in this way to offer a systematic view of the knot lifetime problem. The relevant extensive numerical simulations suggested, among other things, a definite optimization (maximization) of the vortex knot lifetimes for values of λ (the axial vs planar trapping strength) around 1.5–1.6. They also revealed that in the trapped setting, distinct destabilization pathways may arise for the knots. In particular, not only may

*cticknor@lanl.gov
†ruban@itp.ac.ru
‡kevrekid5@gmail.com

they "untie" as they do in the homogeneous setting, but rather portions of the knot can leave the condensate, thus destroying the structure. We now turn to the relevant theoretical setup and the corresponding detailed numerical findings.

II. THEORETICAL SETUP AND NUMERICAL METHOD

The 3D Gross-Pitaevskii equation in trap units[1] takes the dimensionless form

$$i\Psi_t = \big[-\tfrac{1}{2}\Delta + \tfrac{1}{2}(r^2 + \lambda^2 z^2) + g|\Psi|^2 - \mu\big]\Psi, \qquad (1)$$

where $r^2 = x^2 + y^2$. The principal parameters here are the trap anisotropy λ (the ratio between axial and planar trapping strengths) and the interaction strength $g = 4\pi Na/l_r$ with standard unit normalization of the density (however, other appropriate rescaling of Ψ is able to give $g = 1$). Here a is the s-wave scattering length and l_r is the axial oscillator length, equal to $\sqrt{\hbar/m\omega_r}$, where m is the atomic mass and ω_r is the planar trap frequency. The chemical potential μ is assumed sufficiently large (here we typically use $\mu \sim 30$ unless indicated otherwise) in order to ensure the hydrodynamic regime (also referred to as the Thomas-Fermi regime). As a result of this regime, the equilibrium condensate ground state density can be well described by the expression $\rho(z, r) \propto \mu - (r^2 + \lambda^2 z^2)/2$. Thus, the ellipsoid $r^2 + \lambda^2 z^2 = 2\mu$, with transverse size $R_\perp = \sqrt{2\mu}$, is an effective boundary of the condensate at equilibrium, i.e., its density vanishes outside of this ellipsoid. It is common for typical experimental parameters (as discussed, e.g., in [6]) for the relevant timescale to correspond to times of the order of milliseconds. This puts in perspective also the long lifetime of the structures that we will consider below (and which will be on the order of seconds, which is comparable to the lifetime of the condensate).

Following Ref. [50], in the deep Thomas-Fermi limit $\mu \gg 1$ quasistationary vortex torus knots and links $T_{p,q}$ are possible. We have knots when p and q are co-prime integers (including the case $p = 1$ and/or $q = 1$ of trivial knots that can be unfolded to a ring: "unknots") and we have links when $p = np'$ and $q = nq'$, with $n \geqslant 2$ (n knots or rings that are linked together). For example, the well-known trefoil knot is $T_{2,3}$, while the Hopf link is $T_{2,2}$ [52]. All such structures were found theoretically in Ref. [50] to have an equilibrium toroidal radius $R_*(\mu) = \sqrt{2\mu/3}$, and the healing length at that radius is $\xi_* = \sqrt{3/2\mu}$.

The initial (condition for the) position of the vortex core in our studies is assumed to be a distorted torus knot (links are constructed in a similar manner)

$$r(\varphi) + iz(\varphi) = r_0 + r_1 e^{iw\varphi} + \sum_m A_m e^{i(m\varphi/p + \gamma_m)}, \qquad (2)$$

where $w = q/p$ is the winding number, r_0 (r_1) is the toroidal (poloidal) radius, and A_m and γ_m are real amplitudes and phases of perturbations. The latter are needed to break the symmetry of the knot and thus introduce seeds for the development of possible instabilities. Two variants of vortex shape are studied in our numerical experiments: For S1 we use $r_0 = 4.0$ and $r_1 = 0.7$ and for a single m we take $A_m = r_1/20$ and $\gamma_m = 0$, while all the remaining amplitudes are set to zero; for S2 the sum in Eq. (2) is taken over a finite range $q - 10 \leqslant m \leqslant q + 10$, with all-equal A_m's from the set $\{0.001, 0.005, 0.010\}R_*$ and with quasirandom γ_m's uniformly distributed over the interval $[0, 2\pi)$. In case S2 a typical value of the sum is about $5A_m$, which should be compared to $r_1 \sim 0.20R_*$. So $A_m = 0.001R_*$ gives a nearly perfect torus knot, while $A_m = 0.01R_*$ results in significant distortions.

Now to construct the full 3D initial condition we need to specify all of the vortex cores in the (r, z) plane for a given ϕ where there are p vortices; here $r > 0$. We are able to construct the phase of the wave function with the superposition of the phase from each vortex

$$\Psi(\phi, r, z)/\sqrt{|\rho|} = \Pi_j^p \psi_{2D}(r - r_j, z - z_j), \qquad (3)$$

where (r_j, z_j) is the position of the jth vortex core and $\psi_{2D}(r, z) = e^{i\theta}$ with $\theta = \arctan2(r, z)$ where r and z are the distances to a vortex. Thus, the total phase Φ is simply the sum of all the vortex core phases.

Additionally, we use a multistep algorithm to find the initial or ground state of the *trapped* knotted BEC. We arrived at this procedure after trying many different methods of obtaining the initial state, such as only imprinting phase with imaginary time propagation. After much trial and error, the best method we found was to pin the vortex core density and then use imaginary-time propagation. Other procedures (including ones which may work better in homogeneous systems) created significant residual excitations in the initial state of the knot or the BEC's flow around the knot. To be more specific, we perform the following procedures. (i) We imprint the phase of the ground state as found from Eq. (3). (ii) We temporarily introduce an additional pinning potential along the prescribed vortex core. Such a potential is defined by the sum $V(\phi, r, z) = U \sum_j e^{-B\Theta_j}$, where $\Theta_j = (z - z_j)^2 + (r - r_j)^2$ and U and B are suitable coefficients. We concentrate mainly on the two following choices: V1, a relatively smooth pinning with $U = 50$ and $B = 15$; and V2, a sharp pinning with $U = 600$ and $B = 240$. (iii) We have a short but heavily damped imaginary-time propagation corresponding to a dissipative regime. This step allows a relaxation of wave function in the trap that eliminates the most undesirable large-scale sound-mode perturbations [51]. Especially important is the relaxation of the spatial phase distribution to a state where $\mathrm{div}(\rho\nabla\Phi) \approx 0$. Unlike a uniform background with ρ being a constant, in our case ρ depends on $\mathbf{r}$ and so we do not have an analytic tool to determine the equilibrium $\Phi(\mathbf{r})$. That is why the dissipative stage is an efficient practical method to reduce potential modes in the initial state.

It should be noted, however, that despite the pinning, the vortex core still retains some small deviation from the prescribed shape (2) during the dissipative stage. Mainly it is a small increase of r_1, but with our U and B, the deviation is less than vortex core width (the healing length). Another important point is that the relatively smooth pinning (V1) potential results in a fat vortex core at the end of stage (iii). As conservative evolution starts, the core returns quickly to its

[1] In traps the length scale is $l_r = \sqrt{\hbar/m\omega_r}$, where ω_r is the trapping frequency and m is the mass. The energy scale is $\hbar\omega_r$ and the timescale is $1/\omega_r$.

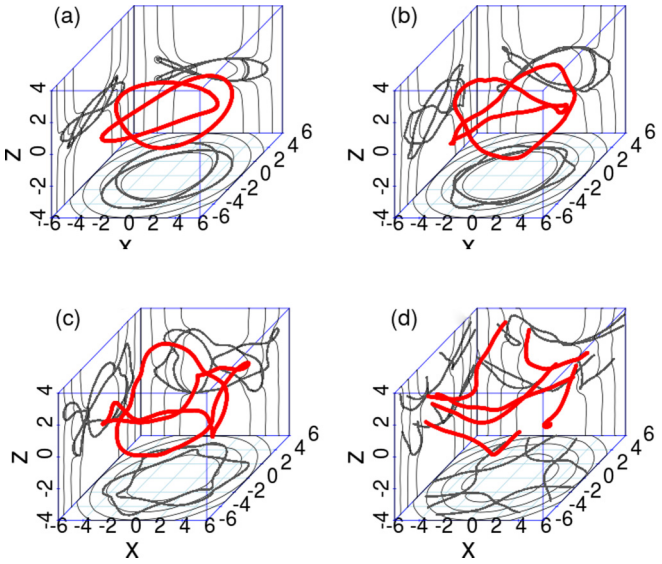

FIG. 1. For $\lambda = 0$ snapshots are shown along the demise of the knot within the BEC. In each panel the extracted vortex cores are shown in red and then in gray lines they are projected on the sides of the image. In addition to the vortex cores, the thin black lines show the density of the BEC on the sides of the image. (a) The initial configuration at $t = 0$, (b) the knot distorts at $t = 15$, (c) portions of the knot further extend outward at $t = 35$, and (d) portions of the vortices leave the volume at $t = 38$. Note that this is not a process that leads to a link being formed as would happen in free space. The axes are in oscillator units $\sqrt{\hbar/m\omega_r}$.

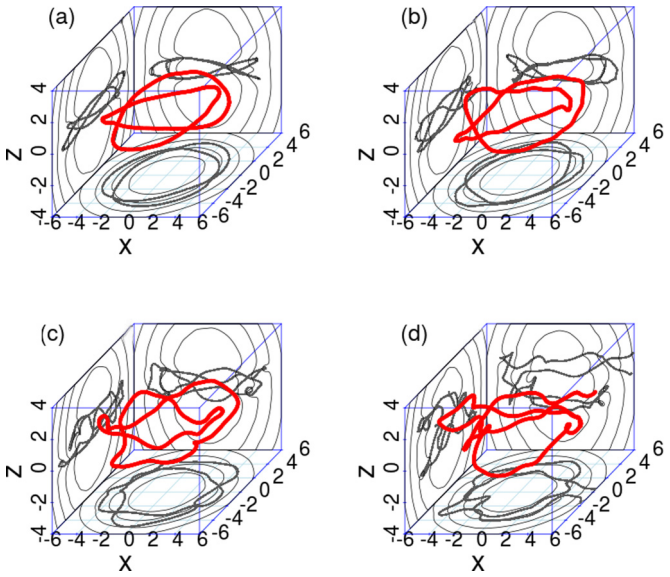

FIG. 2. Snapshots showing the decay of the vortex knot for $\lambda = 0.85$. The evolution already looks very different for $\lambda = 0$. In (a) we see the early form of the knot at $t = 10$; (b) at $t = 25$ some Kelvin-wave-induced undulations arise. (c) At $t = 32.5$ the knot has untied and (d) later at $t = 40$ a loop has left the BEC. The axes are in oscillator units $\sqrt{\hbar/m\omega_r}$.

normal width, thus producing some short-scale nonstationary ripples on the density background. The ripples act then as additional perturbations and reduce the vortex lifetime comparatively to more clean backgrounds corresponding to the sharper pinning potential (V2). However, further sharpening of the pinning potential is not efficient as it is unable to trap the vortex.

The time propagation of Eq. (1) takes place with a third-order operator splitting Fourier spectral method, with time steps of 5×10^{-4}, with a numerical grid of 256^3, and with a spacing of $0.07 l_r$. This method preserves energy at the eighth decimal place for all simulations.

Having provided the setup of our numerical experiments, we now turn to a summary of our extensive numerical investigations.

III. RESULTS

The behavior of a knot in free space has been studied, in particular, in Refs. [37,41]. The basic motion of a trefoil is that the knot rolls over in a regular motion. Eventually the knot will untie as perturbations grow and the regular rolling motion ends [37,41]. We will now examine the behavior of a knot in various geometries, starting with λ equal to 0, 0.85, and then looking at 1.6 and 1.8. We present results for trefoil knots with a single-m perturbation S1 and smooth pinning V1.

In Fig. 1 we show the evolution of a T_{23} knot in a trap with $\lambda = 0$. This is just a tube scenario, involving no confinement in the z direction. The red line is the 3D vortex, i.e., it represents the position of the vortex core. The vortex positions are extracted by finding the phase singularity on the computational grid [53]. We further refine these vortex positions via the method used in Ref. [29,54]. This method offers a subgrid resolution on the position of the vortex core. To be more specific, on a grid plaquette with a vortex core, the grid vertices will have a phase profile like $\Psi \propto e^{i\varphi}$, where φ is the unknown angle measured from the vortex core to the grid points. The phase can be distorted from this, but it does have a 2π phase wrap. This method then seeks to approximate the locations on the edges where the real and imaginary parts of the Ψ go to zero. Then the two points where $\mathrm{Re}[\Psi] = 0$ form a line and the two points where $\mathrm{Im}[\Psi] = 0$ form another line. Where these two lines intersect, we find the vortex core.

Additionally, both the BEC's density (thin black lines) and the extracted cores are projected (gray lines) onto the back planes: (x, y), (x, z), and (y, z). One can discern that early on during the evolution for this scenario the knot gets distorted due to undulations (the so-called Kelvin waves [6,22]). As a result, already at times earlier than 40 in our dimensionless units, the knot has broken into individual undulating filaments, losing its coherence as a trefoil structure. Note this is not a process that leads to a link being formed as would happen in free space. This is one way in which the trap alters the dynamics of the knot. A movie of the simulation is shown in Ref. [55]. The above unconfined along the z-direction scenario can be contrasted with the trapped case along the z direction. In Fig. 2 we show a system with $\lambda = 0.85$. In this case the knot unties, more like the knot's evolution in free space.

The knot is shown at various stages of its evolution with an $m = 4$ perturbation. At $t = 10$ [Fig. 2(a)] we see an early form of the knot, while at $t = 25$ [Fig. 2(b)] the knot has started featuring Kelvin-wave undulations. At $t = 32.5$ [Fig. 2(c)] the knot has untied, and later at $t = 40$ [Fig. 2(d)] a loop has left

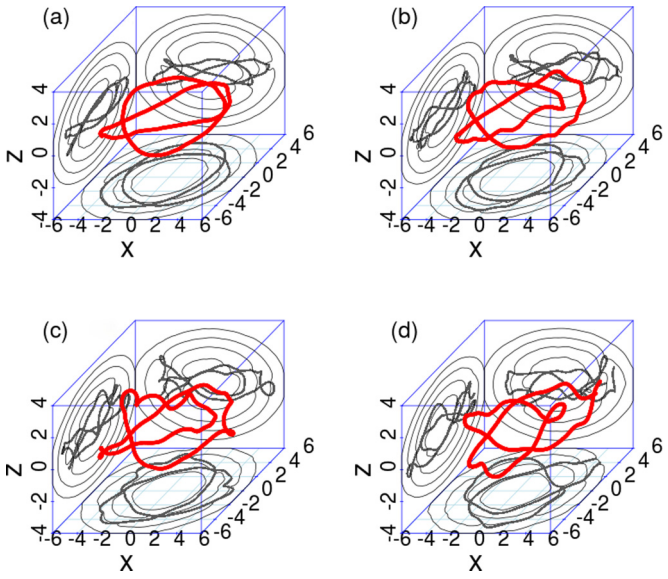

FIG. 3. Snapshots along the demise of the trefoil knot inside the BEC for $\lambda = 1.8$. (a) At $t = 202$ initial distortions appear; (b) at $t = 263$ growth of undulations appears. (c) At $t = 303$ further growth of undulations is shown, while (d) shows the eventual breakup around at $t = 324$ when a portion of the knot leaves the BEC's volume. The axes are in oscillator units $\sqrt{\hbar/m\omega_r}$.

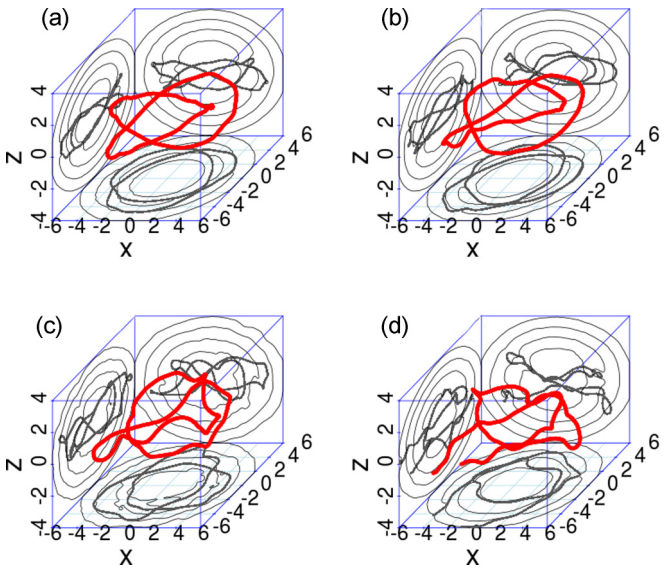

FIG. 4. Snapshots showing the decay of the vortex knot for $\lambda = 1.6$. At (a) $t = 500$ and (b) $t = 1000$ the emergence of nontrivial undulations can be observed, but these remain small. (c) At $t = 1130$ the knot has untied into a link, while (d) at $t = 1153$ a portion of the link is leaving the volume. The axes are in oscillator units $\sqrt{\hbar/m\omega_r}$.

the BEC's volume. For $\lambda = 0.85$ this is fairly typical behavior. With lower m (one, two, or three) perturbations, the knot also tilts like a ring [31] in a trap with $\lambda < 1$, but the knot still unties in a similar fashion. A movie of the simulation is shown in Ref. [55].

In a trap, it is important to highlight that (in addition to untying) there is another way for the knot to decay: Perturbations can grow so large that a portion of the knot can leave the BEC's Thomas-Fermi ellipsoidal confinement region before the knot unties. In Fig. 3 we show the evolution of a T_{23} knot in a trap with $\lambda = 1.8$ with no perturbation $A_m = 0$. Here it can be seen that the evolution retains the coherence of the trefoil for times that are about an order of magnitude longer than $\lambda = 0$ and 0.85.

In Fig. 3(b), already at $t = 263$, the helical Kelvin-like undulations have started forming. These Kelvin modes are the manifestation of small-amplitude imperfections in the initial knot configuration preparation which are amplified over time and eventually give rise to the unstable dynamics observed. These are seen to grow in intensity at $t = 303$ [Fig. 3(c)], where the knot further distorts but still has a trefoil structure. Finally, in Fig. 3(d), at $t = 324$ the structure becomes untied not by becoming a link, but by having a portion leave the volume (i.e., the confinement region discussed above). A movie of the simulation can be found in Ref. [55].

To illustrate the main point of our work, namely, the dramatic impact of judiciously chosen anisotropy on the lifetimes of the vortex knots, we now turn to a case involving $\lambda = 1.6$. In Fig. 4 we show the evolution of a $T_{2,3}$ knot in a trap with this λ. The knot exists over 1100 trap units of time before it unties. Just after the knot unties, it is shown in Fig. 4(c), and then the knot evolves and eventually a portion of the structure leaves the volume in Fig. 4(d). Remarkably, under initialization similar to that in the cases considered above, we observe a lifetime about 4 times larger than in Fig. 3 and nearly 30 times longer than for the case of Fig. 1. It is then clear that a suitable tuning of the anisotropy can endow a knot structure with very long lifetimes, conceivably enabling its experimental observability. A movie of the simulation is in Ref. [55].

To measure the lifetimes of the knot structures, we analyze the extracted core positions within the (approximate Thomas-Fermi) region $0.9R_\perp$. (The 0.9 prefactor is used to avoid ghost vortices from disrupting the knot analysis [29,53].) Then we order the core positions so that they are a continuous function in φ spanning the interval from 0 to $2p\pi$; see Fig. 5(a) for r and Fig. 5(b) for z of the extracted vortex core positions.

When the separation of two points anywhere along the knot exceeds a cutoff distance (larger than the grid spacing), the knot is considered to be broken. This works also for reconnection events as a knot unties. To further the analysis we can extract the toroidal $r_0(t)$, poloidal $r_1(t)$, and z, labeled $z_0(t)$ positions of the vortex in the knot. Using these quantities, we define $\langle z\rangle$ by taking the average of the z_0 coordinate over the entire knot, $\langle z\rangle = 1/N_c \sum_i^{N_c} z_i$, where N_c is the number of vortex core positions found on our grid; $r_0 = \langle r\rangle$ is found in the same fashion. To obtain r_1 at a given time we take $r_1^2 = 1/N_c \sum_i^{N_c} (z_i - \langle z\rangle)^2 + (r_i - \langle r\rangle)^2$. In Fig. 5(c) we show the radial position of the two-vortex cores in a knot for $\phi = 0$ as a function of time. The position of one core is red, while the other is black. We can see their regular motion as they tumble over each other. We can see that r_0 is the average radial position of the knot and r_1 is the distance the two vortices traverse in their rotation about each other. In Fig. 5(d) we show the extracted r_0; note the vertical scale difference of Figs. 5(c) and 5(d).

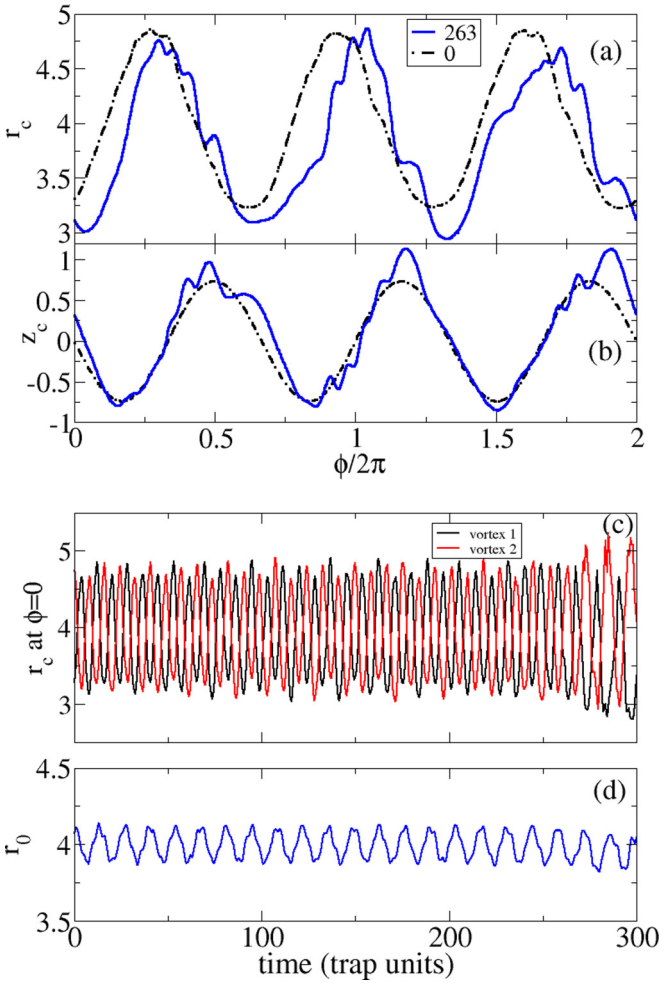

FIG. 5. Plot of (a) r_c and (b) z_c as a function of ϕ for $\lambda = 1.8$, shown at different times 0 (black dash-dotted line) and 263 (blue solid line). These data are extracted from the same simulations shown in Figs. 3(a) and 3(b). (c) For the trefoil, there exist two vortices at each ϕ. Here the radial position of each is shown as a function of time. From these data we extract r_0, r_1, and z. (d) Average toroidal radius r_0 as a function of time. The y axes are in oscillator units $\sqrt{\hbar/m\omega_r}$.

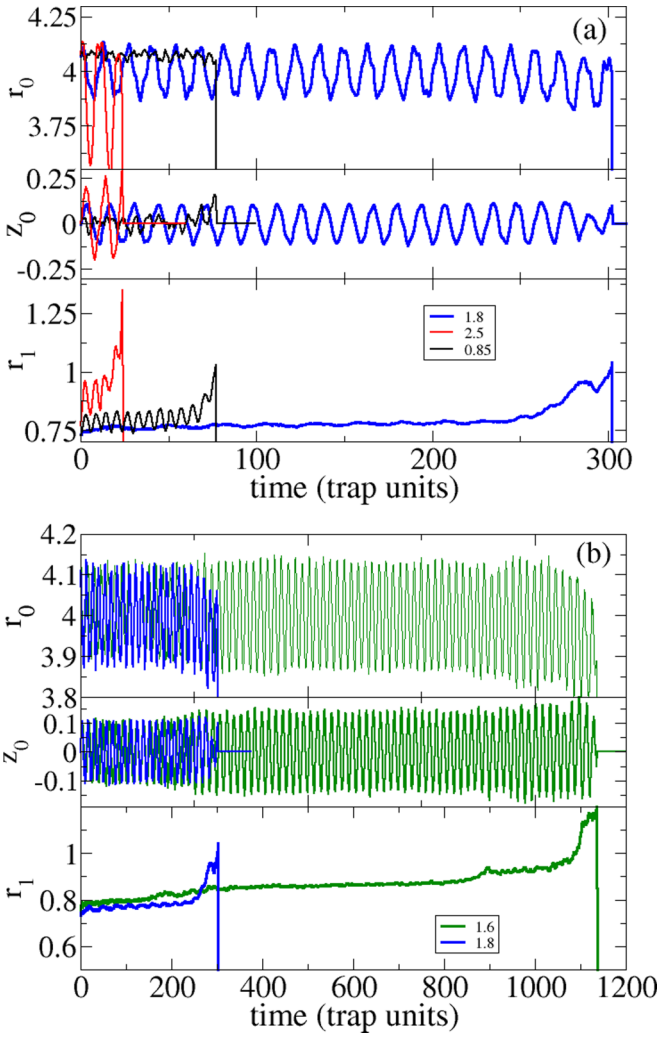

FIG. 6. Extracted effective coordinates r_0 (top), z_0 (middle), and r_1 (bottom) are shown for different λ: (a) $\lambda = 0.85$ (black line), 1.8 (blue line), and 2.5 (red line) and (b) $\lambda = 1.6$ (green line) and 1.8 (blue line). It is important to note the disparity in the timescales of the breakup of the different anisotropy knot structures. The same initial knot and chemical potential were used. When the knots are no longer complete (untie), the curves are set to zero. The y axes are in oscillator units $\sqrt{\hbar/m\omega_r}$.

We contrast the typical evolution of r_0, r_1, and z_0 for different λ's in Fig. 6. In Figs. 6(a) and 6(b) we show the extracted r_0 (top), z_0 (middle), and r_1 (bottom) for many different geometries. In Fig. 6(a) we show the shorter evolution of $\lambda = 0.85$ (red line), 2.5 (black line), and 1.8 (blue line). Then in Fig. 6(b) we compare the long evolution of $\lambda = 1.6$ (green line) and 1.8 (blue line). The main observation here, corroborating the snapshots presented earlier in Figs. 2–4, is that we have a huge variation in the lifetime of trapped knots. In particular, while for prolate or highly oblate condensates the knots are highly unstable [see the black and red curves for $\lambda = 0.85$ and $\lambda = 2.5$ in Fig. 6(a)], it is possible to expand their lifetimes by over a factor of 10 by judiciously tuning the anisotropy towards somewhat oblate condensates, most notably in the case of $\lambda = 1.6$ [green curve in Fig. 6(b)]. We observe nearly 100 rotations of the knot in the $\lambda = 1.6$ case. Interestingly (but also perhaps somewhat intuitively) this also reflects the corresponding earlier observations for the stability in the case of vortex rings which can be thought of as partial constituents of vortex knots. See, e.g., the theoretical analysis of [23], as well as the recent numerical confirmation of [31]. In these works, it was found that for $\lambda < 1$ (i.e., for prolate condensates) the vortex rings are unstable to a tumbling mode. On the other hand, for $2 < \lambda \leqslant 3$ they are unstable due to a quadrupolar Kelvin mode, for $3 < \lambda \leqslant 4$ further destabilized due to a hexapolar Kelvin mode, and so on. Hence, this tighter trapping of the weakly oblate condensates indeed seems to prevent the manifestation of these Kelvin modes for such ring structures. Knots are genuinely three-dimensional objects; hence, eventually, the destabilization due to these modes materializes. However, the geometry of the condensate apparently delays this effect within the interval of $1 < \lambda < 2$.

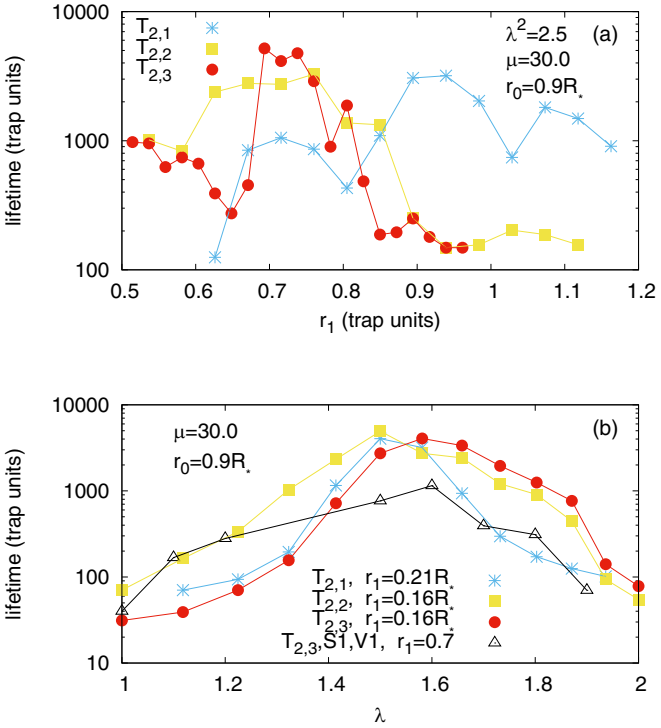

FIG. 7. Lifetimes corresponding to S2 and V2 over (a) the initial poloidal radius r_1 for fixed anisotropy and (b) the anisotropy parameter λ for fixed initial conditions. For comparison, some results for S1 and V1 are also shown. In general, the smoother pinning of the form V1 turned out to be less optimal for long-lived knots.

The oscillations in these quantities (r_0, r_1, and z_0) are related to the excitations of the knot, but also correspond to the knot completing a rotation (see Fig. 5). For most cases we have looked at (except the $\lambda = 0$), the knot breaks in a fashion where the poloidal (effective) coordinate r_1 seems to diverge as a portion of the knot leaves the volume or unties.

Besides that, to more precisely determine the domains of maximal lifetime within the parameter space, we performed several series of simulations with initial states prepared using sharp pinning V2 and multiple-mode perturbations S2 for $A_m = 0.001R_*$. Similarly, we have varied the knot's initial conditions to identify the lifetime dependence on initial conditions, as well as that on the chemical potential. In these simulations, the lifetime was measured until the moment of first reconnection. The results are shown in Fig. 7(a) as lifetime dependences over the initial poloidal torus radius r_1 with a fixed, nearly optimal value of the anisotropy parameter λ and with a fixed, nearly optimal value of the toroidal radius r_0 (it should be noted here that optimal r_0 has been empirically found as approximately $0.9R_*$ at moderately large $\mu \sim 30$, slightly different from the theoretical limit $1.0R_*$). In Fig. 7(b), the lifetimes are plotted versus the anisotropy parameter λ for fixed initial r_1 and r_0. For comparison, analogous results for smooth pinning V1 and single-m perturbation S1 are also shown there. Indeed, distinct parametric intervals can be identified where simple vortex knots, unknots, and links survive over many hundreds of their revolutions. Prototypical examples of each class are offered in Fig. 7. For instance, for $1.4 < \lambda < 1.8$,

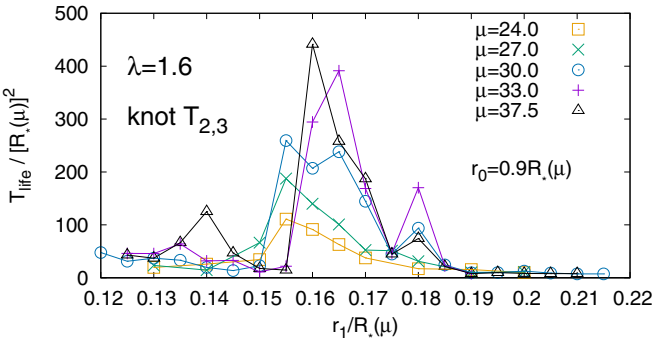

FIG. 8. Normalized trefoil lifetimes for different values of the chemical potential. The tendency towards larger lifetimes can be observed for increased values of μ.

we observe the significant increase of the structure lifetimes [Fig. 7(b)]. A similar feature arises for $0.65 < r_1 < 0.8$, as a function of the initial condition parameter r_1, for fixed λ.

Here it should be mentioned that a control simulation with large perturbation corresponding to $A_m = 0.01R_*$ demonstrated a decrease of the lifetime in the quasistable domain by a factor of roughly 10 (not shown). Moderate perturbation with $A_m = 0.005R_*$ resulted in a lifetime roughly half as long, which is still quite long. Thus, even less accurately prepared vortex knots are able to exist for a long time in suitable parametric regimes, as revealed by our study.

Finally, in Fig. 8 we compare trefoil lifetimes as a function of the ratio r_1/R_*, for different values of chemical potential μ. In this case it is convenient to normalize the results to $R_*^2(\mu)$ in order to separate the overall tendency $T_{\rm life} \sim \mu$. Thus, the normalized lifetime provides a general impression (up to a factor of order 1) about the number of knot rotations before its destruction. We can observe an evident tendency towards an enhanced lifetime for larger values of the chemical potential μ. This result is intuitively natural since a larger μ implies a weaker coupling of the vortical pattern to sound modes.

IV. CONCLUSION

In this work, we have explored the effects of initial condition preparation (through variations of the poloidal coordinate r_1), trap anisotropy (by tuning the confinement ratio λ), and background density or nonlinearity (varying the chemical potential μ) on the lifetime of knot structures in confined atomic Bose-Einstein condensates. Arguably, our most significant finding is that anisotropic traps with (trapping ratios) $\lambda \approx 1.6$ can essentially stabilize (i.e., lead to enhanced lifetimes by over an order of magnitude) torus vortex knots and links in Bose-Einstein condensates with moderate values of the local induction parameter $\Lambda = \ln(R_*/\xi_*) \lesssim 3$. We similarly identified optimal values of r_1 and illustrated the enhanced lifetime for larger chemical potentials μ.

Compared to the evolution of a knot in free space, the lifetimes of a knot in a trap can be many times larger. Proment *et al.* [37] found lifetimes to be about 60 in our trap units. (They found lifetimes to be about 1200 units of time corresponding to a system where the healing length is 1. When rescaled to the same units as we use, these lifetimes

are shorter by a factor $2\mu/3$.) In the present work we observed lifetimes of up to 1000 and even 5000 trap units. Alternatively, we observed many hundreds of vortex turnover times in Fig. 6(b).

We observed that the dynamics leading to the eventual demise of the most-long-lived knots and links involves the sound generation by the rotating vortex structures. This process gradually increases the parameter r_1 "pushing it out" of a quasistable interval. After that Kelvin waves are produced, progressively distorting the knots or links and ultimately leading to their destruction (via either untying or leaving the Thomas-Fermi region). For comparison, recent results based on the Biot-Savart approximation indicate that for vortex knots and links of the same relative sizes in spatially uniform condensates the mechanism of knot destruction is an intrinsic linear instability without stable zones [42,43].

These results offer a systematic understanding of the viability of observation of torus knots in confined atomic condensates. They show how initial condition, trapping, and nonlinear features of the underlying problem may enhance the relevant lifetimes rendering them potentially experimentally accessible (e.g., by combination of techniques such as phase imprinting of elaborate phase patterns as in, e.g., [56], coupled with the painting of suitable pinning potentials as in, e.g., [57]). Moreover, they offer some intuition of the relevant optimality of slightly oblate condensates in connection with corresponding results for vortex rings. This finding is exciting because of recent experimental progress on producing knots in BECs [44,45]. We hope this proposal will aid future studies and searches for trapped vortex knots. Among the important open tasks remaining are of course the experimental realization of such structures via phase (or perhaps density) engineering, but also a realization of these knots as exact solutions of the system from a numerical perspective. In particular, their rotation suggests that they may be exact periodic orbits of the system; hence computationally demanding periodic orbit identification tools may, in principle, be used to find such exact solutions and to assess their stability via, e.g., Floquet theory.

ACKNOWLEDGMENTS

This material is based upon work supported by the U.S. National Science Foundation under Grant No. PHY-1602994 and Grant No. DMS-1809074 (P.G.K.). The work of V.P.R. was supported by the RF Program No. 0033-2019-0003. C.T. acknowledges funding from the Los Alamos National Laboratory, which is operated by Triad National Security, LLC for the Department of Energy under Contract No. 89233218CNA000001.

[1] P. G. Saffman, *Vortex Dynamics* (Cambridge University Press, Cambridge, 1992).
[2] L. M. Pismen, *Vortices in Nonlinear Fields* (Clarendon, Oxford, 1999).
[3] R. J. Donnelly, *Quantized Vortices in Helium II* (Cambridge University Press, Cambridge, 1991).
[4] C. J. Pethick and H. Smith, *Bose-Einstein Condensation in Dilute Gases* (Cambridge University Press, Cambridge, 2002).
[5] L. P. Pitaevskii and S. Stringari, *Bose-Einstein Condensation* (Oxford University Press, Oxford, 2003).
[6] P. G. Kevrekidis, D. J. Frantzeskakis, and R. Carretero-González, *The Defocusing Nonlinear Schrödinger Equation: From Dark Solitons and Vortices to Vortex Rings* (SIAM, Philadelphia, 2015).
[7] A. L. Fetter, Rev. Mod. Phys. **81**, 647 (2009).
[8] A. L. Fetter and A. A. Svidzinsky, J. Phys.: Condens. Matter **13**, R135 (2001).
[9] P. G. Kevrekidis, R. Carretero-González, D. J. Frantzeskakis, and I. G. Kevrekidis, Mod. Phys. Lett. B **18**, 1481 (2004).
[10] S. Komineas, Eur. Phys. J. Spec. Top. **147**, 133 (2007).
[11] C. F. Barenghi and N. G. Parker, *A Primer in Quantum Fluids* (Springer, Berlin, 2016).
[12] A. C. White, B. P. Anderson, and V. S. Bagnato, Proc. Natl. Acad. Sci. USA **111**, 4719 (2014).
[13] A. A. Svidzinsky and A. L. Fetter, Phys. Rev. A **62**, 063617 (2000).
[14] V. P. Ruban, Phys. Rev. E **64**, 036305 (2001).
[15] A. Aftalion and T. Riviere, Phys. Rev. A **64**, 043611 (2001).
[16] J. J. García-Ripoll and V. Pérez-García, Phys. Rev. A **64**, 053611 (2001).
[17] A. Aftalion and R. L. Jerrard, Phys. Rev. A **66**, 023611 (2002).
[18] P. Rosenbusch, V. Bretin, and J. Dalibard, Phys. Rev. Lett. **89**, 200403 (2002).
[19] A. Aftalion and I. Danaila, Phys. Rev. A **68**, 023603 (2003).
[20] A. Aftalion and I. Danaila, Phys. Rev. A **69**, 033608 (2004).
[21] I. Danaila, Phys. Rev. A **72**, 013605 (2005).
[22] A. L. Fetter, Phys. Rev. A **69**, 043617 (2004).
[23] T.-L. Horng, S.-C. Gou, and T.-C. Lin, Phys. Rev. A **74**, 041603(R) (2006).
[24] S. Serafini, M. Barbiero, M. Debortoli, S. Donadello, F. Larcher, F. Dalfovo, G. Lamporesi, and G. Ferrari, Phys. Rev. Lett. **115**, 170402 (2015).
[25] R. N. Bisset, W. Wang, C. Ticknor, R. Carretero-González, D. J. Frantzeskakis, L. A. Collins, and P. G. Kevrekidis, Phys. Rev. A **92**, 063611 (2015).
[26] V. P. Ruban, JETP **124**, 932 (2017).
[27] V. P. Ruban, JETP Lett. **106**, 223 (2017).
[28] S. Serafini, L. Galantucci, E. Iseni, T. Bienaime, R. N. Bisset, C. F. Barenghi, F. Dalfovo, G. Lamporesi, and G. Ferrari, Phys. Rev. X **7**, 021031 (2017).
[29] R. N. Bisset, S. Serafini, E. Iseni, M. Barbiero, T. Bienaime, G. Lamporesi, G. Ferrari, and F. Dalfovo, Phys. Rev. A **96**, 053605 (2017).
[30] W. Wang, R. N. Bisset, C. Ticknor, R. Carretero-Gonzalez, D. J. Frantzeskakis, L. A. Collins, and P. G. Kevrekidis, Phys. Rev. A **95**, 043638 (2017).
[31] C. Ticknor, W. Wang, and P. G. Kevrekidis, Phys. Rev. A **98**, 033609 (2018).
[32] D. H. Wacks, A. W. Baggaley, and C. F. Barenghi, Phys. Fluids **26**, 027102 (2014).
[33] R. M. Caplan, J. D. Talley, R. Carretero-González, and P. G. Kevrekidis, Phys. Fluids **26**, 097101 (2014).

[34] V. P. Ruban, Phys. Fluids **30**, 084104 (2018).
[35] R. L. Ricca, D. C. Samuels, and C. F. Barenghi, J. Fluid Mech. **391**, 29 (1999).
[36] F. Maggioni, S. Alamri, C. F. Barenghi, and R. L. Ricca, Phys. Rev. E **82**, 026309 (2010).
[37] D. Proment, M. Onorato, and C. F. Barenghi, Phys. Rev. E **85**, 036306 (2012).
[38] D. Kleckner and W. T. M. Irvine, Nat. Phys. **9**, 253 (2013).
[39] D. Proment, M. Onorato, and C. F. Barenghi, J. Phys.: Conf. Ser. **544**, 012022 (2014).
[40] P. Clark di Leoni, P. D. Mininni, and M. E. Brachet, Phys. Rev. A **94**, 043605 (2016).
[41] D. Kleckner, L. H. Kauffman, and W. T. M. Irvine, Nat. Phys. **12**, 650 (2016).
[42] V. P. Ruban, JETP Lett. **107**, 307 (2018).
[43] V. P. Ruban, JETP **127**, 581 (2018).
[44] D. S. Hall, M. W. Ray, K. Tiurev, E. Ruokokoski, A. H. Gheorghe, and M. Möttönen, Nat. Phys. **12**, 478 (2016).
[45] W. Lee, A. H. Gheorghe, K. Tiurev, T. Ollikainen, M. Möttönen, and D. S. Hall, Sci. Adv. **4**, 3820 (2018).
[46] F. Maucher, S. A. Gardiner, and I. G. Hughes, New J. Phys. **18**, 063016 (2016).
[47] D. M. Raymer and D. E. Smith, Proc. Natl Acad. Sci. USA **104**, 16432 (2007).
[48] K. Shimokawa, K. Ishihara, I. Grainge, J. D. Sheratt, and M. Vasquez, Proc. Natl. Acad. Sci. USA **110**, 20906 (2013).
[49] J. W. Cirtain, L. Golub, A. R. Winebarger, B. De Pontieu, K. Kobayashi, R. L. Moore, R. W. Walsh, K. E. Korreck, M. Weber, P. McCauley, A. Title, S. Kuzin, and C. E. DeForest, Nature (London) **493**, 501 (2013).
[50] V. P. Ruban, JETP **126**, 397 (2018).
[51] V. P. Ruban, JETP Lett. **108**, 605 (2018).
[52] https://en.wikipedia.org/wiki/Link_(knot_theory).
[53] C. J. Foster, P. B. Blakie, and M. J. Davis, Phys. Rev. A **81**, 023623 (2010).
[54] A. Villois, G. Krstulovic, D. Proment, and H. Salman, J. Phys. A: Math. Theor. **49**, 415502 (2016).
[55] See Supplemental Material at http://link.aps.org/supplemental/10.1103/PhysRevA.99.063604 for movies of BEC simulations.
[56] N. Meyer, H. Proud, M. Perea-Ortiz, C. O'Neale, M. Baumert, M. Holynski, J. Kronjäger, G. Barontini, and K. Bongs, Phys. Rev. Lett. **119**, 150403 (2017).
[57] K. Henderson, C. Ryu, C. MacCormick, and M. G. Boshier, New J. Phys. **11**, 043030 (2009).